A Compact Dual-Band Filtering Patch Antenna Using Step Impedance Resonators

Chin-Yuan Hsieh, Cheng-Hsun Wu, and Tzyh-Ghuang Ma, *Senior Member, IEEE*

***Abstract*—A compact dual-band three-pole Chebyshev filtering patch antenna with orthogonal polarizations in the two bands is developed for 2.4/5.8-GHz ISM-band applications. Step impedance resonators and aperture coupled feed techniques are integrated together to fulfill the goal. The synthesis procedure is discussed using formulation and design curves. The advantages of the proposed design, including harmonic suppression and controllable bandwidth, are verified by experiments. According to the summary table, this dual-band filtering antenna, realized in planar form, shows either a more compact size or improved radiation characteristics when compared with those reported in the open literature.**

***Index Terms*—Dual-band, filtering antenna, patch antenna, step impedance resonator.**

I. Introduction

MODERN wireless systems require highly integrated RF front-ends with the capability of multi-functional operation. Among the components in the RF front-end, the antenna, responsible for transmitting/receiving signals to/from the space, is of great interest if it can be integrated with other core elements. Amplifying/self-oscillating active antennas [1], rectennas [2], and filtering antennas [3]–[9] have been intensively investigated over the past two decades.

The filtering antenna, a direct integration of the antenna and the second-to-the-last component in the RF front-end (i.e., filter), is capable of providing a compact integrated radiating element with sharp frequency selectivity, good harmonic suppression, and controllable bandwidth. Conventional filter synthesis techniques can be applied to synthesize a filtering antenna by replacing the last stage of the filter network with a radiator [3]. In [4], a ground-intruded coupled line resonator is incorporated with a monopole to realize a two-pole compact filtering antenna. A flat-gain filtering antenna is discussed in [5] with annular resonators and a fan-shaped patch.

Nevertheless, most filtering antennas reported to date are restricted to single-band operation, likely a result of the difficulty in fulfilling the required filter specifications in more than one band. This trend, however, apparently contradicts to the evolution of wireless systems in which multi-band operation has become a necessity. In [6], the dual-band antenna and filter sections are developed separately without a fully integrated process. The antenna responses in [7] do not demonstrate the predicted two-pole filtering characteristics by equations. At the expense of a three-dimensional structure, the dual-band filtering antenna in [8] is well-behaved with good radiation characteristics. A planar dual-band filtering antenna using coupled resonators and a rectangular patch in TM_{10} and TM_{30} modes is proposed in [9]. Its peak gain in the low band is only -4 dBi while the size is large. Up to date, developing a dual-band filtering antenna is still quite a challenging task.

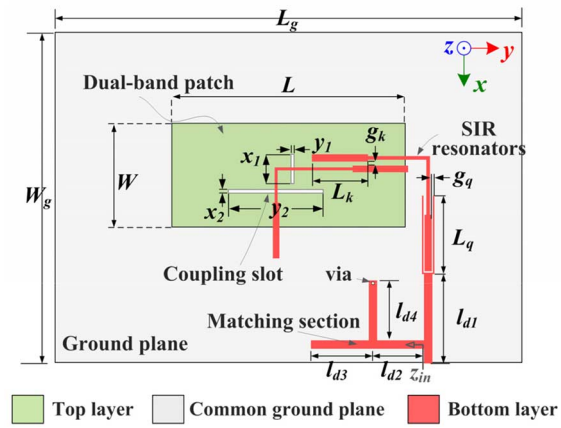

Fig. 1. Geometry of the proposed dual-band filtering patch antenna.

In this letter, by a direct integration of a patch antenna and step impedance resonators (SIRs), a dual-band three-pole Chebyshev filtering antenna is investigated. The antenna, fabricated on a three-layer printed circuit board (PCB), has a patch radiator on the top layer and SIRs on the bottom one. It is fed by spatially orthogonal coupling slots on the common ground plane. The operating principles, synthesis equations, and design graphs are first introduced, followed by experimental results for validation. The advantages of the design, such as higher order mode suppression and bandwidth controllability in both bands, are validated through experiments. A comparison table is summarized to show its performance improvement over the others in terms of either the size or radiation characteristics.

II. Operating Principles

Fig. 1 depicts the layout of the proposed dual-band filtering antenna. The antenna is developed on a three-layer PCB using two stacked 20-mil Roger RO4003 C substrates ($\varepsilon_r = 3.55$ and $\tan\delta = 0.0027$). The patch on the top layer functions not only as a radiating element but also as the third stage of the filter. The second SIR on the bottom layer excites the TM_{10} and TM_{01} modes of the patch respectively in the low and high bands. Aperture coupled feeds with spatial orthogonality are adopted. Unlike the design in [9], exciting the TM_{10} and TM_{01} modes with orthogonal polarizations in the two bands makes the overall design feature a much more compact size. The lengths and widths of the coupling slots (x_1, y_1, x_2, y_2) are chosen to keep good

Manuscript received November 21, 2014; accepted January 04, 2015. Date of publication January 08, 2015; date of current version May 14, 2015. This work was supported by the National Science Council, Taiwan, under Grants 101-2628-E-011-007-MY3 and 102-2221-E-011-011-MY2.

The authors are with the Department of Electrical Engineering, National Taiwan University of Science and Technology, Taipei 10607, Taiwan (e-mail: tgma@mail.ntust.edu.tw; tg.ma@msa.hinet.net).

Color versions of one or more of the figures in this letter are available online at http://ieeexplore.ieee.org.

Digital Object Identifier 10.1109/LAWP.2015.2390033

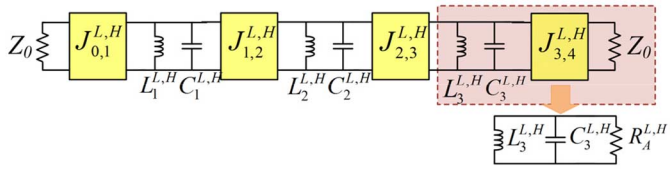

Fig. 2. Lumped three-pole bandpass filter and its one-port equivalence.

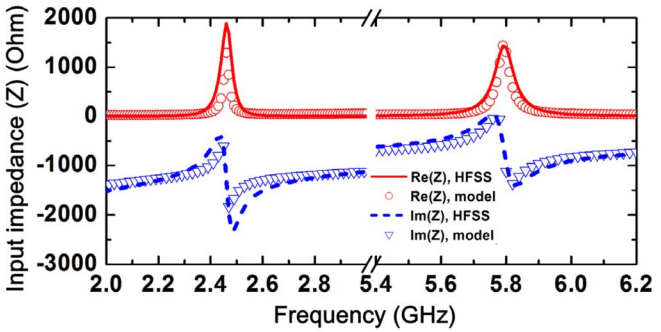

Fig. 3. Model-calculated and full-wave simulated input impedances of the patch antenna in the low and high bands.

matching when the filter sections are removed. The operating frequencies ($f_L = 2.45$ GHz and $f_H = 5.8$ GHz) are respectively determined by the length (L) and width (W) of the patch, which is nearly a half wavelength at the corresponding resonance frequency (TM_{10} and TM_{01}).

Fig. 2 shows the equivalent model of a typical three-pole bandpass filter using lumped LC resonators. To transform the two-port network into a filtering antenna, the output terminal should be first converted to a resistive load $R_A^{L,H}$ using the inverter $J_{3,4}^{L,H}$. Here, the superscripts (L, H) stand for the low and high bands; $R_A^{L,H}$ is in essence the radiation resistance of the antenna. For a standard patch, its radiation resistance in the TM_{10} and TM_{01} modes can be estimated by [10]

$$R_A^{L,H} = 90\frac{{\varepsilon_r}^2}{\varepsilon_r - 1}\left(\frac{l}{w}\right)^2 \tag{1}$$

where l and w are respectively the non-radiating (resonance) and radiating edges. Given $l = L$ and $w = W$ at f_L and $l = W$ and $w = L$ at f_H, the radiation resistances are $R_A^L = 2291\Omega$ and $R_A^H = 86.4\Omega$. The patch antenna near resonance can therefore be modeled by a parallel RLC tank as shown in the lower portion of Fig. 2. While the $R_A^{L,H}$ is calculated from (1), the equivalent inductance and capacitance ($L_3^{L,H}$, $C_3^{L,H}$) are extracted by curve-fitting the impedance response of the lumped RLC model to that derived by a full-wave simulator (HFSS). The extracted values are $L_3^L = 11.7$ nH, $C_3^L = 0.36$ pF, $L_3^H = 0.12$ nH, and $C_3^L = 6.28$ pF. Fig. 3 compares the model-calculated and full-wave simulated antenna input impedances. Good agreement is observed over the band of interest, therefore validating the antenna modeling.

In the SIR, the electrical lengths (θ_L) of the high/low impedance sections are set equal for simplicity. The impedance ratio is selected as $R = 0.611$ to make the first two resonance modes of the SIRs coincided with the TM_{10} and TM_{01} modes of the patch. The corresponding θ_L is 38° at f_L. In the physical layout, the width and length of the high/low impedance lines are (0.4 mm, 8 mm) and (1 mm, 7.5 mm), respectively. The slope parameters of the SIR are extracted as $b_{1,2}^L = 0.078$ at f_L and $b_{1,2}^H = 0.057$ at f_H.

After determining the electrical parameters of the patch antenna and SIRs, the standard filter synthesis technique can be applied to complete the design. For a given filter specification, the J-inverters are

$$J_{0,1}^{L,H} = \sqrt{\frac{b_1^{L,H} FBW^{L,H}}{Z_0 g_0 g_1}} \tag{2}$$

$$J_{j,j+1}^{L,H} = FBW^{L,H}\sqrt{\frac{b_j^{L,H} b_{j+1}^{L,H}}{g_j g_{j+1}}} (j = 1, 2). \tag{3}$$

By converting the J-inverters to external quality factors (Q_e) and coupling coefficients ($\mathrm{M}_{\mathrm{j,j+1}}$), we have

$$Q_e^{L,H} = \frac{b_1^{L,H}}{Z_0 {J_{0,1}^{L,H}}^2} \tag{4}$$

$$M_{j,j+1}^{L,H} = \frac{J_{j,j+1}^{L,H}}{\sqrt{b_j^{L,H} b_{j+1}^{L,H}}}. \tag{5}$$

In (5), the slope parameter of the antenna is $\omega C_3^{L,H}$ as shown in Fig. 2 ($b_3^L = 0.006$ and $b_3^H = 0.229$).

TABLE I
EXTERNAL Q AND COUPLING COEFFICIENTS $\mathrm{M}_{\mathrm{J,J+1}}$

	Q_e	$M_{1,2}$	$M_{2,3}$
f_L (2.45 GHz)	12.7	0.064	0.060
f_H (5.8 GHz)	20.8	0.038	0.039

III. Filter Specifications and Design Graphs

In this letter, the dual-band filtering antenna is developed based on a three-pole Chebyshev lowpass prototype with 0.01-dB passband ripple ($g_0 = g_4 = 1$, $g_1 = g_3 = 0.6292$, $g_2 = 0.9703$). It covers the 2.4/5.8-GHz ISM bands with fractional bandwidths (FBWs) of 5% and 3%, respectively. The required external quality factors (Q_e) and coupling coefficients ($\mathrm{M}_{j,j+1}$) are calculated using (1)–(5) and summarized in Table I. To fulfill the design specifications, the Q_e and $\mathrm{M}_{\mathrm{j,j+1}}$ should be equal to the values listed in the table simultaneously in both bands. To this end, design graphs between adjacent stages are first obtained using the full-wave simulator HFSS. The curves are summarized in Figs. 4–6.

Fig. 4 shows the external quality factor ($Q_e^{L,H}$) versus the gap width (g_q) and coupling length (L_q) of the forked section between the input port and first SIR. To meet $Q_e^L = 12.7$ and $Q_e^H = 20.8$, g_q and L_q are selected as 0.15 and 10.7 mm. The coupling coefficients ($\mathrm{M}_{1,2}$) between the first and second SIRs are shown in Fig. 5. The SIRs are bended to feed the aperture coupled patch antenna properly. With the need of $\mathrm{M}_{1,2}^L = 0.064$ and $\mathrm{M}_{1,2}^H = 0.038$, the gap width ($g_\mathrm{k}$) and overlapped length (L_k) between the SIRs are compromised as 0.55 and 13.2 mm. In the low band, the second stage is somewhat undercoupled while it becomes slightly overcoupled in the high band. Fig. 6 depicts the coupling coefficients ($\mathrm{M}_{2,3}$) between the second SIR and the patch antenna. The tuning of the coupling coefficient is realized by adjusting the location of the coupling slots on the ground plane with respect to the midpoint of the SIR. By setting $L_{\mathrm{OS,L}} = 0.24$ mm and $L_{\mathrm{OS,H}} = 5.75$ mm, $\mathrm{M}_{2,3}{}^L = 0.06$ and $\mathrm{M}_{2,3}^H = 0.039$ are achieved as indicated in the figure.

IV. Experimental Results

The filtering antenna is realized by a direct integration of the three stages as a whole. The final dimensions (in mm) are W

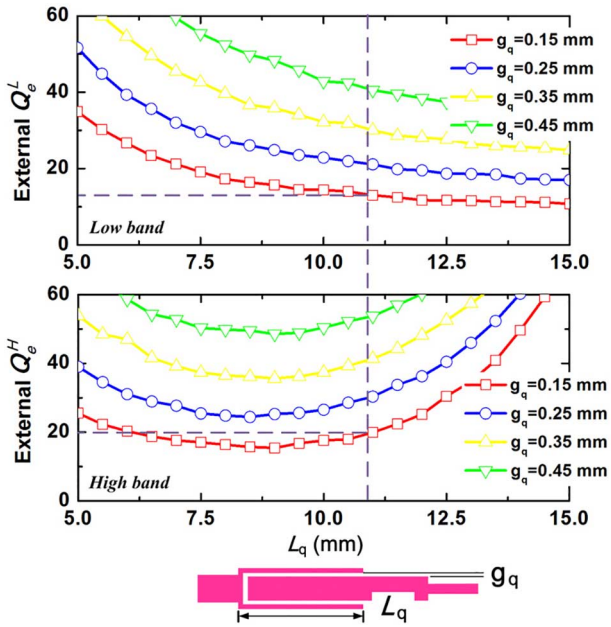

Fig. 4. External Q versus the gap width (g_q) and coupling length (L_q) of the forked coupling section in the low and high bands.

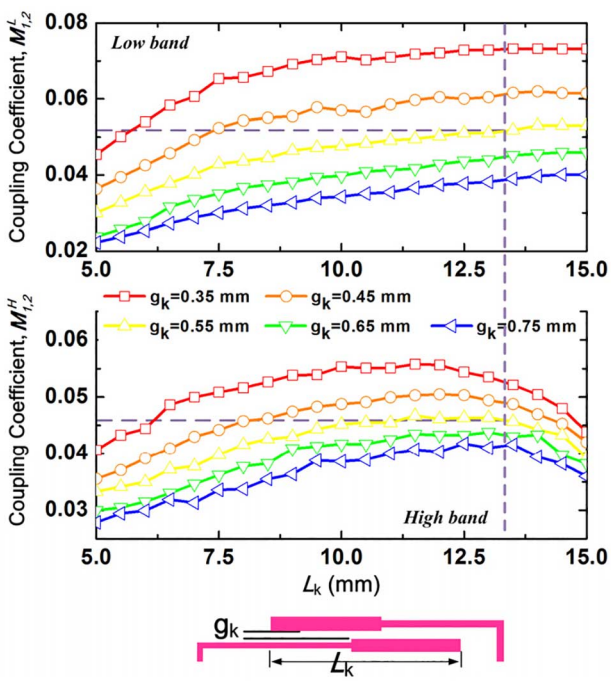

Fig. 5. Coupling coefficient $M_{1,2}$ versus the gap width (g_k) and overlapped length (L_k) between the SIRs in the low and high bands.

$= 14.1$, $L = 32$, $W_g = 45$, $L_g = 64$, $x_1 = 4$, $y_1 = 0.4$, $x_2 = 0.5$, $y_2 = 13$, $g_q = 0.15$, $L_q = 10.7$, $g_k = 0.55$, $L_k = 13.2$, $L_{OS,L} = 0.24$, and $L_{OS,H} = 5.75$. The size of the antenna, including the ground plane, is 45×64 mm^2. To compensate for the undercoupled second stage in the low band, a matching network with open/short stubs is added to the input terminal (Fig. 1). The input impedance looking into the stub ($z_{in,}$) is inductive for matching purpose in the low band, but becomes infinite (o.c.) in the high band to avoid disturbing the already matched antenna system. The dimensions of the stubs are $l_{d1} = 12.2$, $l_{d2} = 7$, $l_{d3} = 8.5$, and $l_{d4} = 8.2$. The operating principle and design equations of the matching section are straightforward; they are omitted for brevity.

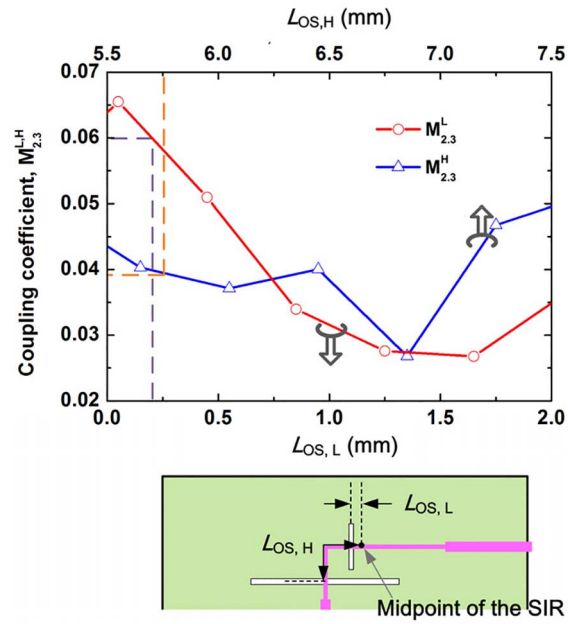

Fig. 6. Coupling coefficient $M_{2,3}$ versus the locations of the coupling slots in the low and high bands.

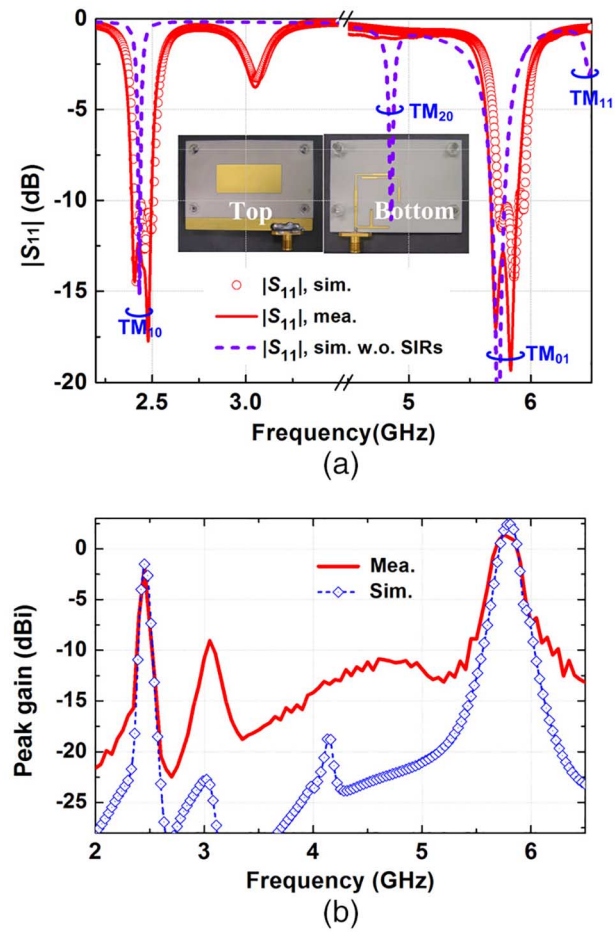

Fig. 7. (a) $|S_{11}|$ and (b) peak gain of the proposed dual-band filtering antenna; simulated $|S_{11}|$ without SIRs is shown for comparison.

The filtering antenna was fabricated and experimentally verified. The simulated and measured input reflection coefficients ($|S_{11}|$) are shown in Fig. 7(a); the simulated $|S_{11}|$ with the patch fed directly without using SIRs is given for comparison purpose. A photograph of the fabricated sample is shown as an

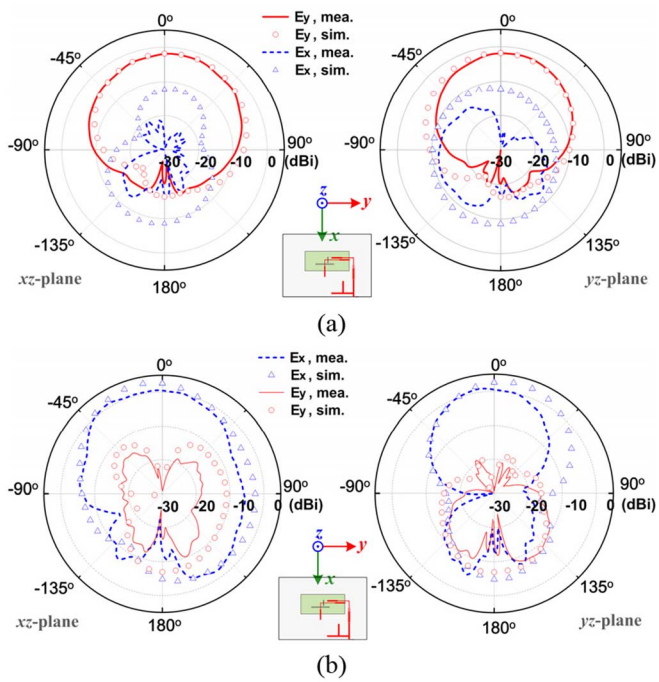

Fig. 8. Simulated and measured radiation patterns in the *xz*- and *yz*-planes in the (a) low band and (b) high band.

inset. The simulated and measured results are in good agreement. Clearly, higher order modes of the stand-alone patch antenna are successfully suppressed. The three-pole filtering antenna also shows sharp frequency selectivity in both bands. The in-band reflection poles can be easily observed, hence validating the design procedure. The measured fractional bandwidths, with $|S_{11}| < -10$ dB, are 4.5% and 3.8%.

The simulated and measured peak gains are summarized in Fig. 7(b). Reasonable agreement is observed. The gains and radiation patterns were measured in an anechoic chamber using the NSI 700S-90 spherical near-field scanner from Nearfield Systems Inc. The peak gains at 2.45 and 5.8 GHz are respectively -1.8 and 1.1 dBi. Due to the scattering from background clutters, the measured gain level in the stopband is an order higher than that in the simulation. Nevertheless, except for the spurious resonance at 3.1 GHz, the peak gain is kept lower than -10 dBi over the frequency band of concern. The spurious resonance is likely a result of the parasitic monopole mode of the SIRs and matching network on the bottom layer. In the simulation, the radiation leakage from this parasitic resonance is below -20 dBi and becomes negligible. In the measurement, however, due to the long testing cable, the effective unbalanced current path is extended such that its peak gain is boosted to -9 dBi. Adding defected ground structures could be a way to further alleviate the spurious radiation.

Fig. 8(a) and (b) compares the simulated and measured radiation patterns in the principal planes. Like a conventional patch, the radiation is broadside in both bands. The co-polarized electric fields in the low (TM_{10}) and high (TM_{01}) bands are orthogonal to each other. In reality, this is believed not to be a fatal issue since the transmitting-receiving antenna pair in ISM bands can barely be kept in perfect alignment.

Finally, Table II compares the operating principle and performances of the proposed dual-band filtering antenna with those reported in the open literature [6]–[9]. Benefitting from the unique excitation scheme (TM_{10} and TM_{10}), this planar filtering antenna provides a good compromise between the

TABLE II
PERFORMANCE SUMMARY OF DUAL-BAND FILTERING ANTENNAS

	f_L, f_H (GHz)	FBW (%)	Peak Gain (dBi)	Size (mm^2)	Order of filter	Process/Approach
[6]	2.5; 5.5	28%; 10%	n.a.	n.a.	4-pole	2-layer PCB/ Monopole+SIR
[7]	1.95; 2.14	1.85%; 1.5%	-1.45; -2.09	25 × 18	2-pole*	2-layer PCB/ Slot+interdigital C
[8]	2.45; 5.5	4%; 7.5%	0.99; 4.83	36 × 15.4 × 6 mm	2-pole	3D structure/ DRA+monopole+SIR
[9]	2.45; 5.2	4.5%; 5.5%	-4.0; 4.0	140 × 140	2-pole	2-layer PCB/ Patch+SIR
This work	2.45; 5.8	4.5%; 3.8%	-1.8; 1.1	45 × 64	3-pole	3-layer PCB/ Patch+SIR

n.a.: not reported.

* reveals single-pole responses.

electrical parameters and circuit size. When compared with that in [9] (TM_{10} and TM_{30}), its low-band gain is improved whereas the size is significantly reduced. The proposed filtering antenna does not require a three-dimensional dielectric resonator antenna as that in [8]. The performance improvement of the proposed idea is clearly demonstrated.

V. CONCLUSION

By utilizing spatially orthogonal aperture coupled feeds and step impedance resonators, a dual-band three-pole filtering patch antenna is proposed and experimentally verified in this letter. The synthesis procedure and design graphs are investigated in detail. This filtering patch antenna demonstrates good harmonic suppression along with controllable passband bandwidth using filter synthesis equations. Profiting from the unique feed structure with spatially orthogonal radiated fields in the two bands, the proposed design outperforms its conventional counterparts in terms of either the size or radiation characteristics. Further improving the gain of the filtering antenna would be an interesting topic worthy of future study.

REFERENCES

[1] K. Chang, R. A. York, P. S. Hall, and T. Itoh, "Active integrated antennas," *IEEE Trans. Microw. Theory Tech.*, vol. 50, no. 3, pp. 937–944, Mar. 2002.

[2] T. Sakamoto, Y. Ushijima, E. Nishiyama, M. Aikawa, and I. Toyoda, "5.8-GHz series/parallel connected rectenna array using expandable differential rectenna units," *IEEE Trans. Antennas Propag.*, vol. 61, no. 9, pp. 4872–4875, Sep. 2013.

[3] C.-T. Chuang and S.-J. Chung, "Synthesis and design of a new printed filtering antenna," *IEEE Trans. Antennas Propag.*, vol. 59, no. 4, pp. 1036–1042, Mar. 2011.

[4] C.-T. Chuang and S.-J. Chung, "A compact printed filtering antenna using a ground-intruded coupled line resonator," *IEEE Trans. Antennas Propag.*, vol. 59, no. 10, pp. 3630–3637, Oct. 2011.

[5] X.-W. Chen, F.-X. Zhao, L.-Y. Yan, and W.-M. Zhang, "A compact filtering antenna with flat gain response within the passband," *IEEE Antennas Wireless Propag. Lett.*, vol. 12, pp. 857–860, 2013.

[6] D. Zayniyev and D. Budimir, "Dual-band microstrip antenna filter for wireless communications," in *IEEE Int. Symp. Antennas and Propagation Digest*, 2010.

[7] H. Kanaya, K. Hayakawa, Y. Nagata, D. Kanemoto, K. Yoshida, R. Pokharel, K. Yoshitomi, A. Ishikawa, S. Fukagawa, and A. Tahira, "Development of dual band miniaturized slot antenna with 2-stage bandpass filter," in *IEEE Int. Symp. Antennas and Propagation Digest*, 2011, pp. 2761–2764.

[8] U. Naeem, S. Bila, S. Verdeyme, M. Thévenot, and T. Monédière, "A compact dual band filter-antenna subsystem for 802.11 wi-fi applications," in *Proc. Eur. Wireless Technology Conf.*, 2010, pp. 181–184.

[9] Y.-J. Lee, G.-W. Cao, and S.-J. Chung, "A compact dual-band filtering microstrip antenna with the same polarization planes," in *Proc. Asia-Pacific Microw. Conf.*, 2012, pp. 1178–1180.

[10] J. D. Kraus and R. J. Marhefka, *Antennas*, 3rd ed. New York, NY, USA: McGraw-Hill, 2001.